JOURNAL OF THEORETICAL AND APPLIED MECHANICS
48, 3, pp. 579-604, Warsaw 2010

NEURO-WAVELET DAMAGE DETECTION TECHNIQUE IN BEAM, PLATE AND SHELL STRUCTURES WITH EXPERIMENTAL VALIDATION

Magdalena Rucka
Krzysztof Wilde

Gdansk University of Technology, Faculty of Civil and Environmental Engineering, Gdańsk, Poland
e-mail: mrucka@pg.gda.pl; wild@pg.gda.pl

The paper presents a new neuro-wavelet damage detection technique for structural health monitoring. The proposed method combines the ability of the continuous wavelet transform to detect abnormalities in the structure dynamic parameters with the artificial neural network possibility of learning, remembering and recognition. The effectiveness of the method is verified on experimental mode shapes of a beam, plate and shell structures. The results of the study show that the neural network trained on the data from a simple structure can effectively improve the search of the location of the same type of damage in complex structures.

Key words: damage detection, continuous wavelet transform, artificial neural networks

1. Introduction

All structures raised by humans wear out and undergo self-destruction in the course of time. Fatigue, corrosion, dynamic phenomena, overloading and environmental conditions can cause their degradation. In order to improve the reliability and safety of structures, various damage detection techniques and health monitoring systems have been intensively studied over the last few decades. A simple, quick and nondestructive structural diagnostic system that could facilitate traditional diagnostic procedures is of great importance for solving many problems with maintenance of engineering structures.

A relatively recent area of research in damage detection and localization is based on the continuous wavelet transform (CWT). This technique can be performed on mode shapes or static deflections of structure elements. An important feature of the wavelet transform is the ability to characterize the local

irregularity introduced by a defect and to react to subtle changes of the structure response. Most of the reported research, e.g., Douka *et al.* (2003), Hong *et al.* (2002) is limited to crack identification by wavelets in beams. Only a few studies (Wang and Deng, 1996; Douka *et al.*, 2004; Chang and Chen, 2004) are devoted to damage detection in plate structures based on numerically determined data. The experimental researches on plate damage detection were presented by Rucka and Wilde (2005). The experimental mode shapes of the cantilever plate were determined by the acceleration measurement in one point and impact excitation in 66 points. The relative depth of the introduced rectangular defect was 19%. The location of the damage was determined by the one-dimensional Gaussian wavelet with 4 vanishing moments. The formulation of the two-dimensional continuous wavelet transform for plate damage detection was presented by Rucka and Wilde (2006a). Damage localization by the Reverse Biorthogonal wavelet on the experimental mode shapes of a plate with four fixed supports was proposed. In the presented research, the location of the peak in the response indicated the damage location in the structure. However, in the case of the experimental data contaminated by noise, the precise identification of the wavelet peaks becomes possible only for serve damage. In Fig. 1a the wavelet transform of the beam static deflection line (cf. Rucka and Wilde, 2006b) for the crack of the relative depth of 50% is shown. In this case, the localization of the damage is easy and precise. Although, the decision of damage location in the case of the crack depth of 35% (Fig. 1b) cannot be drawn without doubts.

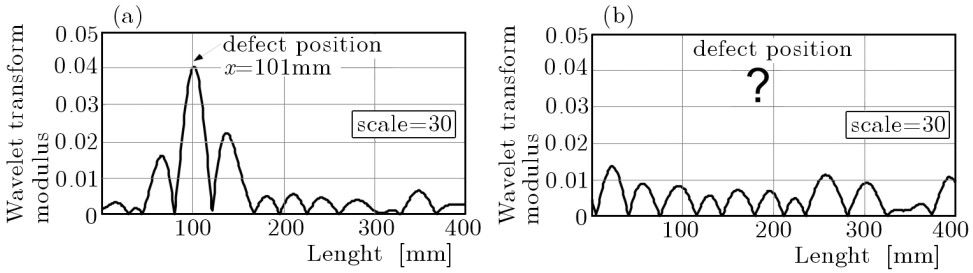

Fig. 1. Experimental wavelet transform modulus of the beam deflection lines: (a) visible defect position, (b) hidden defect position

Damage detection schemes can be enhanced by the use of the artificial neural networks (ANN). In earlier studies, damage recognition and localization based on the ANN were applied to different structures like ships (Zubaydi *et al.*, 2002) or helicopters (Cabell *et al.*, 1998), crates of beverages (Zacharias *et al.*, 2004), joints in steel structures (Yun *et al.*, 2001), bridges (Barai and

Pandey, 1997; Yeung and Smith, 2005). From among many types of artificial neural networks the backpropagation neural network is the most commonly used to the analysis of civil engineering problems (Kuźniar and Waszczyszyn, 2002; Hoła and Schabowicz, 2005). In the previous studies, as inputs of ANN were used: the ultrasonic signals (Liu *et al.*, 2002; Okafor and Dutta, 2001), broad-band spectral signals (Garg *et al.*, 2004), natural frequencies (Sahin and Shenoi, 2003; Waszczyszyn and Ziemiański, 2001; Zapico *et al.*, 2003) or vibration responses (Barai and Pandey, 1997; Kao and Hung, 2003; Yam *et al.*, 2003). Sanz *et al.* (2007) as well as Yam *et al.* (2003) applied wavelet transforms of vibration signals as inputs to ANN.

In this study, the wavelet transforms of static deflection lines as well as the wavelet transforms of vibration mode shapes are used to the search of damage localization. The artificial neural network is trained and tested on a simple cantilever beam with a rectangular notch on static deflection lines. Then the method is validated on the experimentally determined first three mode shapes of the beam, plate and shell with damage of similar type. The possibility of enhancing the very simple peak-picking method by an artificial neural network is studied.

2. Damage detection strategy of the neuro-wavelet system

The practical application of the neuro-wavelet (NW) system for a real engineering structure is practically impossible since the training of the NW system requires data of the structure with a large number of damage combinations. On existing structures in use, there is very limited space for extensive static or dynamic tests, not to mention the possibility of imposing damage in a large number of locations. Therefore, the notion of derivation of the NW system on very simple tests is hereafter presented.

It is proposed that the data from the static experiments on a simple cracked cantilever beam facilitated by the numerical data obtained from updated FEM models is sufficient to define the NW system for monitoring the complex structures. It is expected that the NW system can detect damage regardless of the structure geometry and the type of the measurements. It is assumed that the defect geometry is the same in all considered structures.

The wavelet transform moduli computed from the measurement signals are used as inputs to the neural network system. The advantage of the wavelet transform over the Fourier transforms or measurement records is the ability to extract the selected information from the various types of signals. Thus,

it is possible to combine, for example, the data from static experiments with the data from dynamic tests. The disadvantage of wavelets is the problem with selection of the most appropriate waveform and its number of vanishing moments. The choice of the best wavelet function usually requires trial and error simulations.

The proposed NW system is intended to have the ability of recognizing two levels of damage detection precision, namely, the presence of damage and its position. The search of damage presence and prediction of damage position is considered independently. If the NW system gives the information that there is no damage in the structure, the results on damage location are neglected. Based on the Authors' experience, various experimental data transformed by wavelets contains information with different intensity. For example, the mode shapes extracted from the ambient vibrations (Wilde *et al.*, 2006) might not be sufficiently precise to indicate the damage location, but are good for drawing the conclusion on damage presence.

The cantilever beam of plexiglass with the rectangular cross-section is considered as the simple testing structure. The data for the NW system training are obtained form the static tests conducted on the beam with a defect. In this paper, a rectangular notch obtained by a cut by a high precision saw is considered as the defect. The static deflection lines for different damage configuration were determined by a photogrametric method (cf. Rucka and Wilde, 2006b). The NW system training data also consist of the numerical static deflection lines of the beam. Although the experiments on the cantilever beam are very simple, it is still complicated to test all possible defects positions and defect depths. Therefore, the results from the experimentally verified FEM model of the cracked beam are employed. In the training data the "noise free" as well as the deflection lines with added noise are used. Next the NW system is verified on the experimental mode shapes of the beam, plate and shell structures.

The neural part of the NW system is a simple two hidden layer artificial neural network (Fig. 2). The procedure of damage prediction in the complex structure consists of the following stages:

1. Find the mode shapes of the monitored structures.
2. Calculate the wavelet transform moduli of the mode shapes.
3. Feed the CWT moduli to the NW system.
4. Evaluate the output regarding defect presence (0 means there is no defect, 1 means defect exists).
5. Evaluate output regarding defect localization (0 means there is no defect, x_i denotes the defect position).

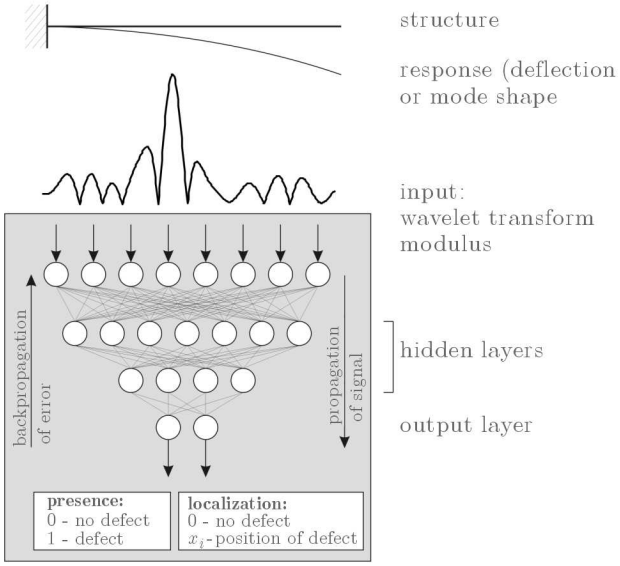

Fig. 2. Outline of the neuro-wavelet damage detection system

3. Continuous wavelet transform in damage detection

For a given one-dimensional signal $f(x)$, the continuous wavelet transform (CWT) can be obtained by integration of the product of the signal function with the complex conjugate $\psi^*(x)$ of the wavelet functions. Considering the deflection line or mode shape of the structures as a one-dimensional signal $f(x)$, the continuous wavelet transform can be defined as (e.g. Mallat, 1998)

$$Wf(u,s) = \frac{1}{\sqrt{s}} \int_{-\infty}^{+\infty} f(x)\psi^*\Big(\frac{x-u}{s}\Big)\, dx \tag{3.1}$$

$Wf(u,s)$ is called the wavelet coefficient for the wavelet $\psi_{u,s}(x)$ and it measures the variation of the signal in the vicinity of the position u whose size is proportional to the scale s. In detection of signal singularities, the vanishing moments play an important role. A wavelet has n vanishing moments if it carries out the following condition

$$\int_{-\infty}^{+\infty} x^k \psi(x)\, dx = 0 \qquad k = 0, 1, 2, \ldots, n-1 \tag{3.2}$$

A wavelet with n vanishing moments can be rewritten as the n-th order derivative of a smoothing function $\theta(x)$. The resulting wavelet transform can be expressed as a multiscale differential operator

$$Wf(u,s) = s^n \frac{d^n}{du^n}(f(x)^* \overline{\theta}_s(x))(u) \qquad \overline{\theta}_s(x) = \frac{1}{\sqrt{s}}\theta\Big(\frac{-x}{s}\Big) \tag{3.3}$$

where $f(x) * \overline{\theta}_s(x)$ denotes convolution of functions and can be interpreted as an average of $f(x)$ over a domain proportional to the scale s. Thus wavelet transform is the n-th derivative of the signal $f(x)$ smoothed by the function $\overline{\theta}_s(x)$ at the scale s. The singularities are detected by finding the abscissa where the maxima of the wavelet transform modulus $|Wf(u,s)|$ converge at fine scales (Mallat, 1998).

The selection of an appropriate type of wavelet and the choice of its number of vanishing moments is essential for effective use of the wavelet analysis. The use of wavelets that create the maximum number of wavelet coefficients that are close to zero is proposed. For the first mode shape of a cantilever or simply supported beam, wavelets with 4 vanishing moments should be used. For structural responses that are similar to a polynomial of higher order than 4, the use of wavelets with a higher number of vanishing moments is necessary. In this paper, the Gaussian wavelets gaus4 and gaus6 having four and six vanishing moments, respectively, have been chosen as the best candidates to damage detection with the one-dimensional continuous wavelet transform. The advantage of the Gaussian wavelets was discussed by Gentile and Messina (2003), Mallat (1998) as well as Rucka and Wilde (2006b, 2007).

In the case of the plate mode shape, i.e. two-dimensional spatial signal $f(x,y)$, the two-dimensional wavelet transform of the function $f(x,y)$ is given by (Rucka and Wilde, 2006a)

$$\begin{aligned} W^i f(u,v,s) &= \frac{1}{s}\int_{-\infty}^{\infty}\int_{-\infty}^{\infty} f(x,y)\psi^i\Big(\frac{x-u}{s},\frac{y-v}{s}\Big)\,dx\,dy = \\ &= \frac{1}{s} f * \psi^i\Big(\frac{-u}{s},\frac{-v}{s}\Big) = f * \overline{\psi}^i_s(u,v) \qquad i=1,2 \end{aligned} \tag{3.4}$$

where the horizontal wavelet $\psi^1(x,y)$ and the vertical one $\psi^2(x,y)$ are constructed with separable products of the scaling ϕ and wavelet function ψ

$$\psi^1(x,y) = \phi(x)\psi(y) \qquad \psi^2(x,y) = \psi(x)\phi(y) \tag{3.5}$$

However, in this approach, the number of vanishing moments is the same in both directions. In fact, the two-dimensional wavelet transform is not favourable for the more complicated plate mode shapes, which can be interpolated by polynomials of different order in both directions. Therefore, instead of (3.4) we use one-dimensional integrals

$$W^1 f(u,v,s) = \frac{1}{\sqrt{s}} \int_{-\infty}^{\infty} f(x,y)\psi^*\Big(\frac{y-v}{s}\Big)\, dy$$
$$W^2 f(u,v,s) = \frac{1}{\sqrt{s}} \int_{-\infty}^{\infty} f(x,y)\psi^*\Big(\frac{x-u}{s}\Big)\, dx \tag{3.6}$$

Integration in $(3.6)_1$ is performed for each column of the signal $f(x,y)$ and integration in $(3.6)_2$ is performed for each row of the signal $f(x,y)$. Coefficients $W^1 f(u,v,s)$ and $W^2 f(u,v,s)$ are called horizontal and vertical, respectively, and they are used to formulate the modulus of the wavelet transform at the scale s

$$Mf(u,v,s) = \sqrt{|W^1 f(u,v,s)|^2 + |W^2 f(u,v,s)|^2} \tag{3.7}$$

Note that formula (3.6) indicates independent treatment of the horizontal and vertical coefficients, and therefore, the choice of the number of vanishing moments has to satisfy Eq. (3.2) independently for each direction. In this paper, three mode shapes of the plate fixed at four edges are considered. To analysis of the first mode shape, gaus4 wavelet having four vanishing moments was applied in both directions. Analysis of the second and third mode shapes was conducted using gaus4 wavelet along the plate width, and gaus6 wavelet along the plate length. The additional advantage of applying the two-dimensional wavelet transform in terms of one dimensional integrals is the possibility of using Gaussian wavelets, which do not have scaling functions $\phi(x)$.

4. Artificial neural network

4.1. Architecture and backpropagation algorithm

The used neural network (Fig. 3) consists of three layers – two hidden layers and one output layer. This model includes an input vector $\boldsymbol{z}$, weight

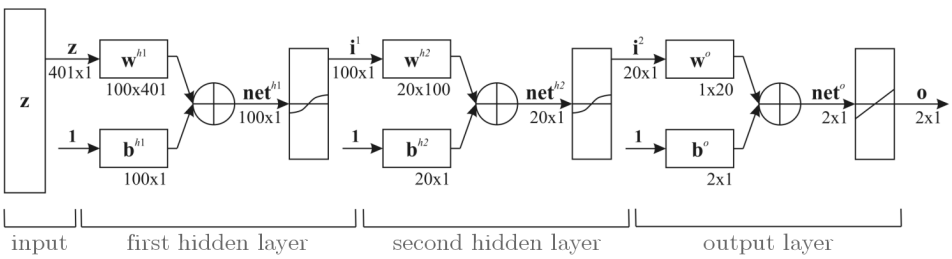

Fig. 3. Architecture of the applied neural network

vector $\boldsymbol{w}$, bias $\boldsymbol{b}$ and output vector $\boldsymbol{o}$. A hyperbolic tangent sigmoid function was selected for the hidden layers and a linear transfer function was selected for the output layer. The input of the neural network is a 401-elements vector of wavelet coefficients. The first hidden layer has 100 neurons whereas the second hidden layer has 20 neurons. These numbers were chosen by trial and error simulations and the previous experiences. The outputs indicate both, the presence and position of the structural defect.

The backpropagation algorithm is explained in details in many sources, e.g. Bow (2002), Hu and Hwang (2002). The net function for the hidden layer neurons and net function for the output layer neurons are given in the form

$$net_m^{h(p)} = \sum_{r=1}^{R} w_{mr}^h z_r^{(p)} + b_m^h \qquad net_k^{o(p)} = \sum_{m=1}^{M} w_{km}^o i_m^{(p)} + b_k^o \tag{4.1}$$

where R and M denote the number of neurons in the input and hidden layers, respectively. The superscript p refers to the p-th input pattern and b is the bias. The input from the m-th hidden layer neuron $i_m^{(p)}$ to the output layer neuron is given as a sigmoid function, whereas the output for the output layer neurons $o_k^{(p)}$ is given as an identity function. The error minimized by the training algorithm is defined as

$$E^{(p)} = \frac{1}{2}\sum_{k=1}^{K}(d_k^{(p)} - o_k^{(p)})^2 \tag{4.2}$$

where K denotes the number of neurons in the output layer and $d_k^{(p)}$ is the known target. The global error can be expressed as a sum of errors of all patterns

$$E = \sum_{p=1}^{P} E^{(p)} \tag{4.3}$$

The weight update equations for both output and hidden layers are given in the form

$$w_{km}^o(t+1) = w_{km}^o(t) - \eta\frac{\partial E^{(p)}}{\partial w_{km}^o} \qquad w_{mr}^h(t+1) = w_{mr}^h(t) - \eta\frac{\partial E^{(p)}}{\partial w_{mr}^h} \tag{4.4}$$

where t is the iteration step and η denotes the learning rate assumed as the same on all neurons in all layers. In this study, the search for the optimal weights is conducted by the scaled conjugate gradient algorithm developed by Moller (1993). The optimization is performed along the conjugate direction, which provides generally faster convergence than the direction of the gradient

steepest descent. The step size is modified at each iteration. This algorithm avoids the time consuming line-search per learning iteration.

To overcome the overfitting problem, the regularization was used. Overfitting means that the error on the training data has a very small value but the error is large on the new simulated data. The performance function, chosen as the mean sum of squares of the network errors

$$mse = \frac{2E}{P} \tag{4.5}$$

is modified by adding a term that consists of the mean of the sum of squares of the network weights and biases (Demuth and Beale, 2003)

$$msereg = \gamma mse = (1-\gamma)msw \tag{4.6}$$

where γ is the performance ratio and msw can be written as

$$msw = \frac{1}{n}\sum_{j=1}^{n} w_j^2 \tag{4.7}$$

It is difficult to determine the optimum performance parameter since too large parameter γ provides overfitting, whereas too small parameter provides no fit in the training data. In the performed tests, the ratio γ was set to 0.5.

Additionally, the correlation coefficient R was used. The correlation coefficient R is a normalized measure of the strength of the linear relationship between the target and predicted value

$$R = \frac{\sum_{i=1}^{P}(o_i - \overline{o})(d_i - \overline{d})}{\sqrt{\sum_{i=1}^{P}(o_i - \overline{o})^2}\sqrt{\sum_{i=1}^{P}(d_i - \overline{d})^2}} \tag{4.8}$$

where o_i and d_i are the output and target values, and $\overline{o}$ and $\overline{d}$ denote mean values. The perfectly correlated data result in a correlation coefficient equal to 1, whereas no correlation results in R equal to 0.

4.2. Training of NW system

The NW system has been trained on the experimental, numerical and noise corrupted numerical data. The training was conduced for the cantilever beam (see Fig. 6a) of length $L = 400\,\text{mm}$, height $H = 20\,\text{mm}$ and width $B = 60\,\text{mm}$ (Rucka and Wilde, 2006b). The beam had one notch of length $L_r = 2\,\text{mm}$ and depth a equal to 7, 10 and 13 mm. In the numerical simulations, the defect location L_1, described by the distance from the clamped end, changed

from 80 mm to 320 mm with step of 4 mm, giving 61 different defect positions. The numerical deflection lines were computed by SOFiSTiK and the noise added to the data had Gaussian distribution with standard deviation changing from 0.02% to 0.05% of the maximum amplitude of the deflection line. In the experimental research, the notch position was $L_1 = 101$ mm. The experimental static deflection lines were obtained in 81 points by the fast photogrammetric technique based on digital photo and image processing (Rucka and Wilde, 2006b). The experimental program is described in Table 1. Beam case 4 from Table 1 was used to the training process.

Table 1. Beam static deflection lines: experimental program

Case No.	Dimensions of beam			Size of defect	
	length L [mm]	heigh H [mm]	width B [mm]	length L_r [mm]	heigh a [mm]
1	400	20	60	0	0
2				2	7
3				2	10
4				2	13

The wavelet transform modulus of the numerical and experimental deflection lines was calculated using gaus4 wavelet for scales 10, 20, 30 and 40. The total number of input patterns was 748. The ANN was trained on the wavelet transform moduli, which clearly indicated damage location, as well as the wavelet transform moduli that did not explicitly point the damage position.

To speed up the ANN learning process, the search of the weights and biases has been divided into five stages. The weights and biases computed in one stage have been used as the initial values for the following stage. In Stage 1, the initial ANN parameters have been randomly selected and the ANN training has been conducted only on the numerical data. Then, to obtain ANN insensitive to noise, the experimental data have been fed (Stage 2) and in Stage 3 all the input patterns have been used. The calculated weights and biases have been slightly corrected on the experimental data (Stage 4) and the final tuning has been done on the noisy numerical wavelet coefficients. The training was stopped either when the error *msereg* achieved 10^{-3} or for a maximum of 700 epochs. The proposed stages of the ANN selection process are the result of the compromise between the search for the minimum calculation time and the best ANN performance (highest correlation coefficient R).

The NW system performance for the best network, with the best recognition ability, is presented in Fig. 4. On the horizontal axis the actual values

are introduced, whereas on the vertical axis they describe the neural network predictions. It can be seen that all points lie very near the line called the best linear fit. The correlation coefficient is 0.99989 and is very close to 1, which indicates very good compatibility between the outputs and targets.

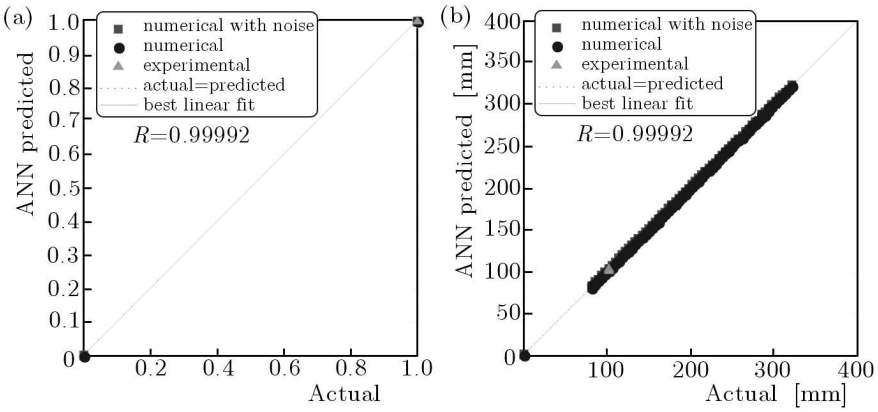

Fig. 4. Results of the training mode; (a) crack presence, (b) crack localization

4.3. Testing of NW system

The wavelet transform moduli, computed for the experimentally determined static deflection profiles (cases 1, 2 and 3 from Table 1), were tested in the trained NW system. Additionally, the numerical patterns were tested. The set of numerical data (noisy and noise-free) was prepared for different defect positions. The distance L_1 from the clamped end to the notch was changed with sampling distance 4 mm, from 82 mm to 318 mm giving 60 different defect locations. The set of numerical data consisted of 488 patterns. Defect localizations in the numerical data of the testing mode were different from the defect localizations in the numerical data of the training mode. However, the predicted values are in good agreement with the actual values. The correlation coefficient reaches 0.99986.

The results of the testing mode are illustrated in Fig. 5. The detailed values for the experimental data are contained in Table 2. It can be noted that the wavelet transform is not able to recognize whether the defect exists or not, in cases 1 and 2. The ANN prediction for the defect presence was -0.0018 for the beam without notch, what means no defect. For beam case 2, the ANN value for the defect existence was 0.9925, what is in agreement with the target value equal to 1. For beam case 3, where the wavelet transform recognized the notch presence, the ANN prediction also confirms this result with the value

0.9976. The maximum error between the actual and predicted values of the defect presence is 0.65%.

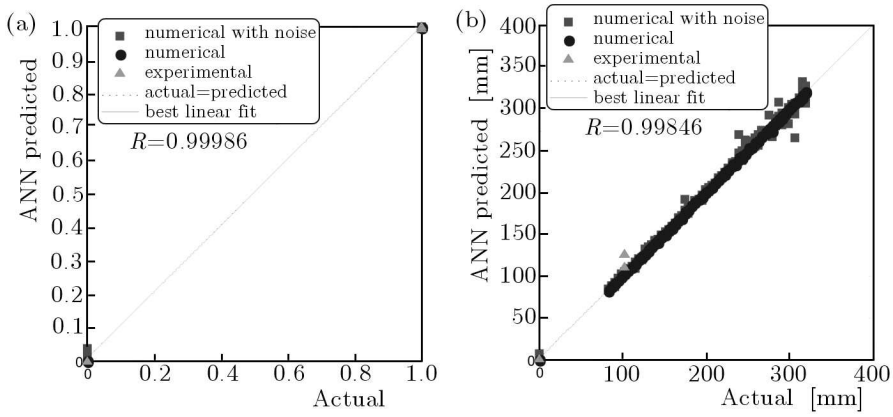

Fig. 5. Results of the testing mode for the beam deflection lines; (a) crack presence, (b) crack localization

Table 2. Actual, recognized by wavelets and neurally predicted defect identification

Input patterns	Patterns description	Defect presence			Defect centre position [mm]		
		Actual	Recognized by CWT	Predicted by ANN	Actual	Recognized ny CWT	Predicted by ANN
case 1	gaus4 $s=30$	0	–	−0.0018	0	–	−0.1449
case 2		1	–	0.9935	101	–	124.6851
case 3		1	1	0.9976	101	101	109.7300

The NW system enabled to predict defect localization for the beam without defect as well as for the beams with defect. The differences are from 8.64% to 23.15%. It can be concluded that the neural network can predict the defect location even if the wavelet transform moduli are not legible (case 1 and 2).

5. Validation of neuro-wavelet system on experimental examples

5.1. Experimental investigations

Experimental tests have been performed on beam, plate and shell structures (Fig. 6). The cantilever beam of length L, width B and height H mm is

made of polymethyl methacrylate (PMMA). The beam contains an open notch of length L_r mm and depth a mm at a distance L_1 from the clamped end. The depth of the defect is 35% of the beam height. The steel plate of length L, width B and height H has a fixed support on each side. The plate contains a rectangular defect of length L_r, width B_r and depth a. The distance from the defect left-down corner to the plate left-down corner in horizontal and vertical directions are L_1 and B_1, respectively. The area of the flaw amounts to 2.4% of the plate area and the depth of the flaw is 25% of the plate height. The cylindrical shell of diameters $D_1 = 293$ mm and $D_2 = 300$ mm is made of steel. The cylindrical shell is welded to a steel plate. The surface area of the cylinder is given in Fig. 6c. The length of the surface is denoted by L, width by B and height by H. The shell contains a rectangular defect of length L_r, height H_r and depth a. The defect is situated from the inside of the cylinder. The distance from the defect left-down corner to the shell left-down corner in horizontal and vertical direction are L_1 and H_1, respectively. The area of the flaw amounts to about 0.2% of surface area and the depth of the flaw is about 30% of the shell thickness. Descriptions of structure geometry, defect sizes and locations as well as experimentally determined material properties are given in Table 3.

Table 3. Beam, plate and shell mode shapes: experimental program

Type of structure	Dimensions of structure [mm]			Size of defect [mm]			Material properties			Location of defect [mm]	
	L	B	H	L_r	B_r	a	E [GPa]	ν [–]	ρ [kg/m^3]	L_1	B_1
beam	480	60	20	2	20	7	3.42	0.32	1187	120	–
plate	560	480	2	80	80	0.5	192	0.25	7430	200	200
shell	930	180	3.4	5	60	1	190	0.25	7850	285	60

The experimental setup of the beam and plate was presented by Rucka and Wilde (2006a). In this paper, the experiments, including the shell structure, are conduced with more advanced signal processing techniques and a noise robust method for the estimation of frequency response functions (FRFs). The structures were subjected to a dynamic pulse load applied by the modal hammer PCB 086C03 at selected points. In the case of the beam, 48 measurement points were distributed along the length of the beam axis whereas in the case of the plate, 143 measurement points were distributed on its surface. The measurement points on the shell were spread out along the central ring and its number amounted to 62. To record the response of the structure one B&K

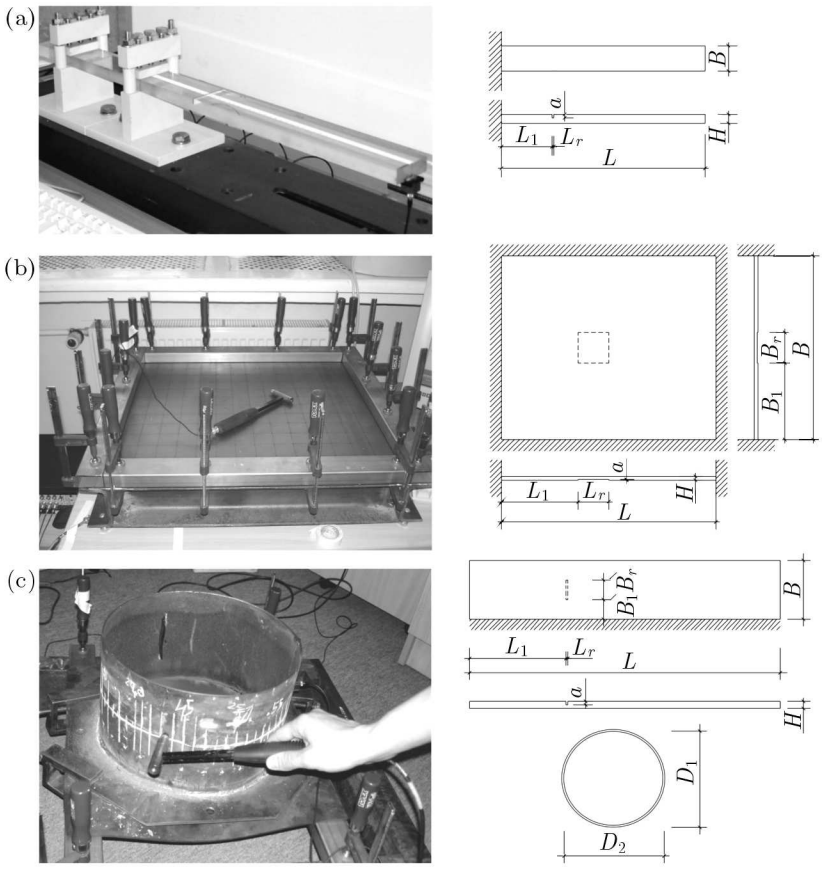

Fig. 6. Experimental setup: (a) beam; (b) plate; (c) shell

accelerometer was used. It was kept in one position throughout the measurements. The acceleration and force data were collected by the data acquisition system Pulse type 3650C. Each acceleration and force measurement was repeated five times and the data were averaged in the frequency domain. The $H_2(\omega)$ estimator was applied to minimize the noise problem in the input signal from modal hammer. The imaginary part of the FRF estimator $H_2(\omega)$ for the beam, plate and shell, is presented in Fig. 7. The obtained FRFs allowed precise identification of the first, second and third mode shapes for all the considered structures.

The mode shapes for the beam, plate and shell were also computed by the commercial FEM program SOFiSTiK. The beam mode shapes were computed using a solid six-sided element of length 2 mm. A square plane element of the size 40×40 mm was used to calculate plate mode shapes. The mode shapes of the shell were computed using a plane element of SOFiSTiK of size 5×5 mm.

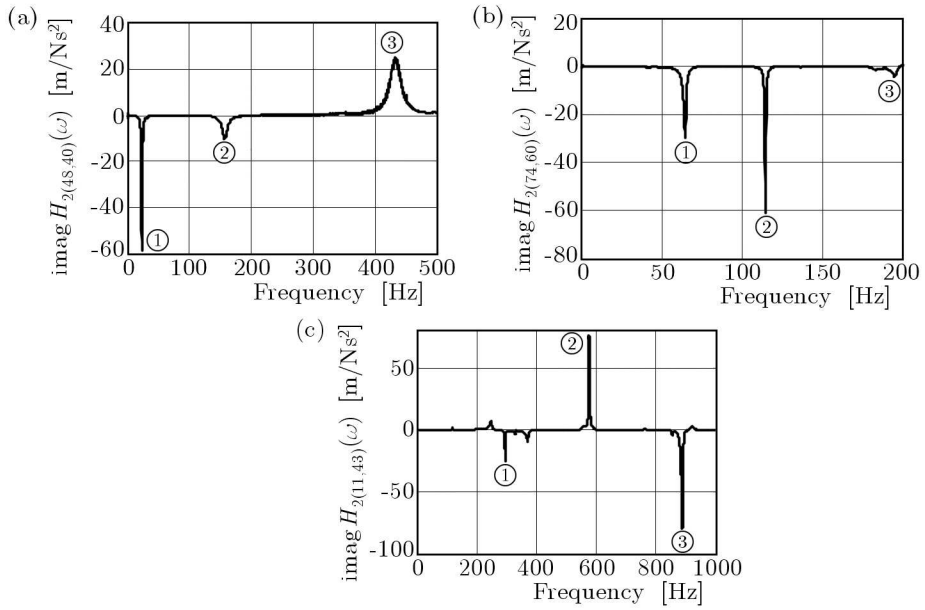

Fig. 7. Imaginary part of FRF estimator $H_2(\omega)$: (a) beam, ① – $f_{1_{exp}} = 23.375\,\text{Hz}$, $f_{1_{num}} = 23.01\,\text{Hz}$; ② – $f_{2_{exp}} = 157.5\,\text{Hz}$, $f_{2_{num}} = 149.91\,\text{Hz}$; ③ – $f_{3_{exp}} = 433.00\,\text{Hz}$, $3_{2_{num}} = 410.89\,\text{Hz}$; (b) plate, ① – $f_{1_{exp}} = 64.875\,\text{Hz}$, $f_{1_{num}} = 65.10\,\text{Hz}$; ② – $f_{2_{exp}} = 114.875\,\text{Hz}$, $f_{2_{num}} = 120.00\,\text{Hz}$; ③ – $f_{3_{exp}} = 195.25\,\text{Hz}$, $3_{2_{num}} = 207.09\,\text{Hz}$; (c) shell, ① – $f_{1_{exp}} = 295.4\,\text{Hz}$, $f_{1_{num}} = 337.3\,\text{Hz}$; ② – $f_{2_{exp}} = 575.8\,\text{Hz}$, $f_{2_{num}} = 614.6\,\text{Hz}$; ③ – $f_{3_{exp}} = 877.2\,\text{Hz}$, $3_{2_{num}} = 928.9\,\text{Hz}$

Numerical frequencies are compared with the experimental ones in the plots of FRFs (Fig. 7). The difference between the measured frequencies relative to calculated frequencies ranges from 0.35% to 12.42%. The experimental and numerical mode shapes are compared in Figs. 8, 9 and 10 for the beam, plate and shell, respectively. Most visible differences between the experimental and numerical modes come form the modelling of the boundary condition. For example, the experimental modes of the beam show some rotation on the support while the numerical model assumes an ideal cantilever beam. Nevertheless, the MAC values range from 0.7411 to 0.9998 indicating a very good agreement.

5.2. Wavelet analysis of structural mode shapes

The continuous wavelet transforms are applied to structural mode shapes. For analysis of beam mode shapes, one-dimensional CWT was used. The wavelet analysis of the first mode shape is performed using gaus4 wavelet having

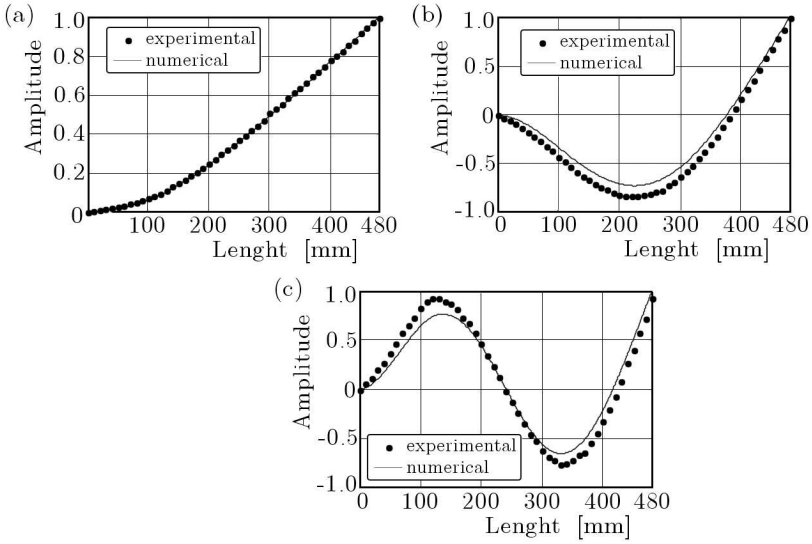

Fig. 8. Experimental and numerical beam mode shapes: (a) first, (b) second, (c) third

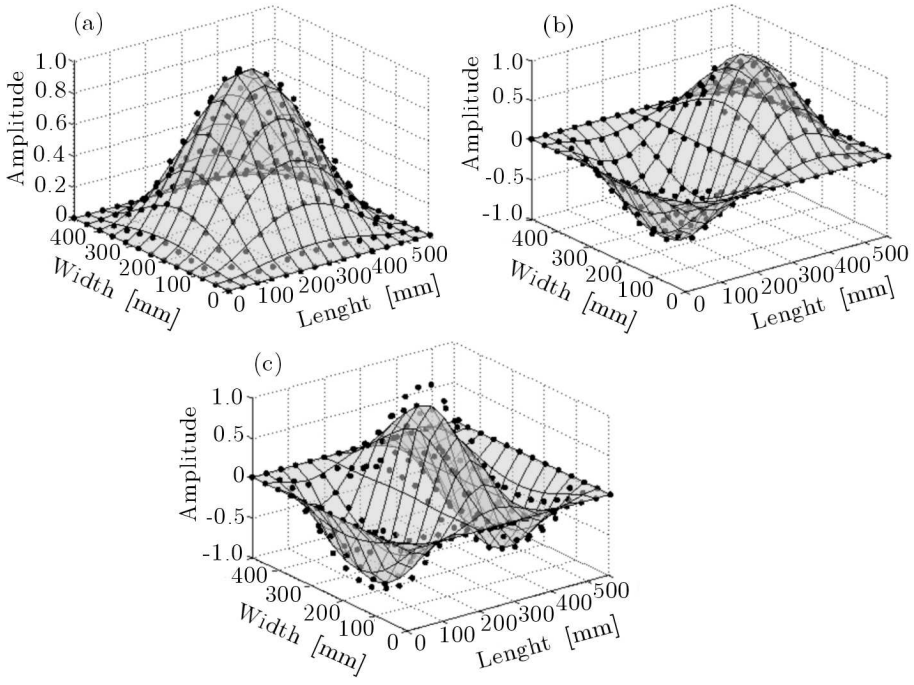

Fig. 9. Experimental and numerical plate mode shapes: (a) first, (b) second, (c) third

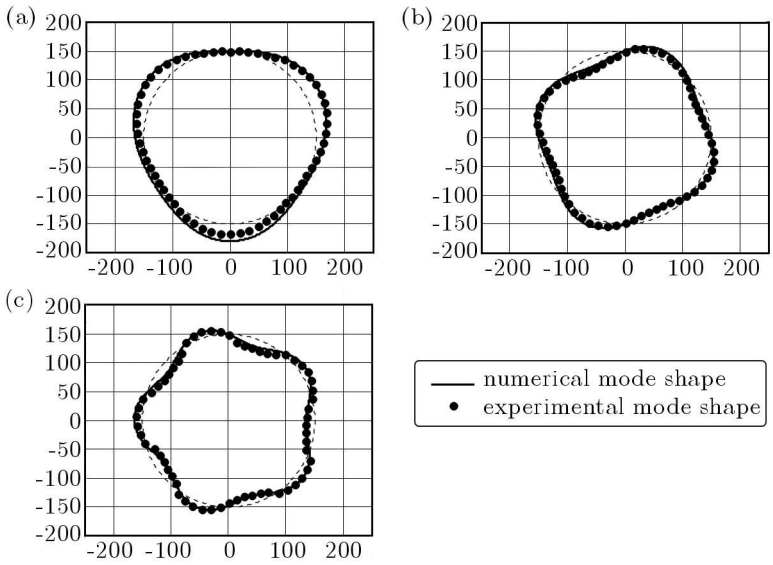

Fig. 10. Experimental and numerical shell mode shapes: (a) first, (b) second, (c) third

4 vanishing moments, whereas the second and third mode shapes are analyzed using gaus6 wavelet having 6 vanishing moments.

The wavelet transform modulus computed for the numerical and experimental data are shown in Fig. 11. In the numerical simulations, the maximum value of the modulus grows with the increase of the scale and clearly points to the defect position at 121 mm from the clamped end. However, the experimental results have additional maxima lines resulting from the measurement noise. Nevertheless, it is possible to locate the damage position, since the dominant maximum line increases monotonically and for larger scales achieves the largest values. The position of the defect determined by wavelet analysis is 132 mm in the case of the first mode shape and 129 mm in the case of the second mode. The wavelet analysis of the third mode shape makes it impossible to detect damage presence and its localization.

The plate analysis was conducted using two-dimensional wavelet analysis expressed in terms of one-dimensional integrals. The presence of the defect is detected by a sudden change in a spatial variation of the transformed response. The wavelet transform moduli for the numerical and experimental data are given in Fig. 12. The results are computed for scale $s = 40$. Analysis of the first mode shape was conducted using gaus4 wavelet in both directions. Both peaks in the wavelet transform modulus for the numerical and experimental

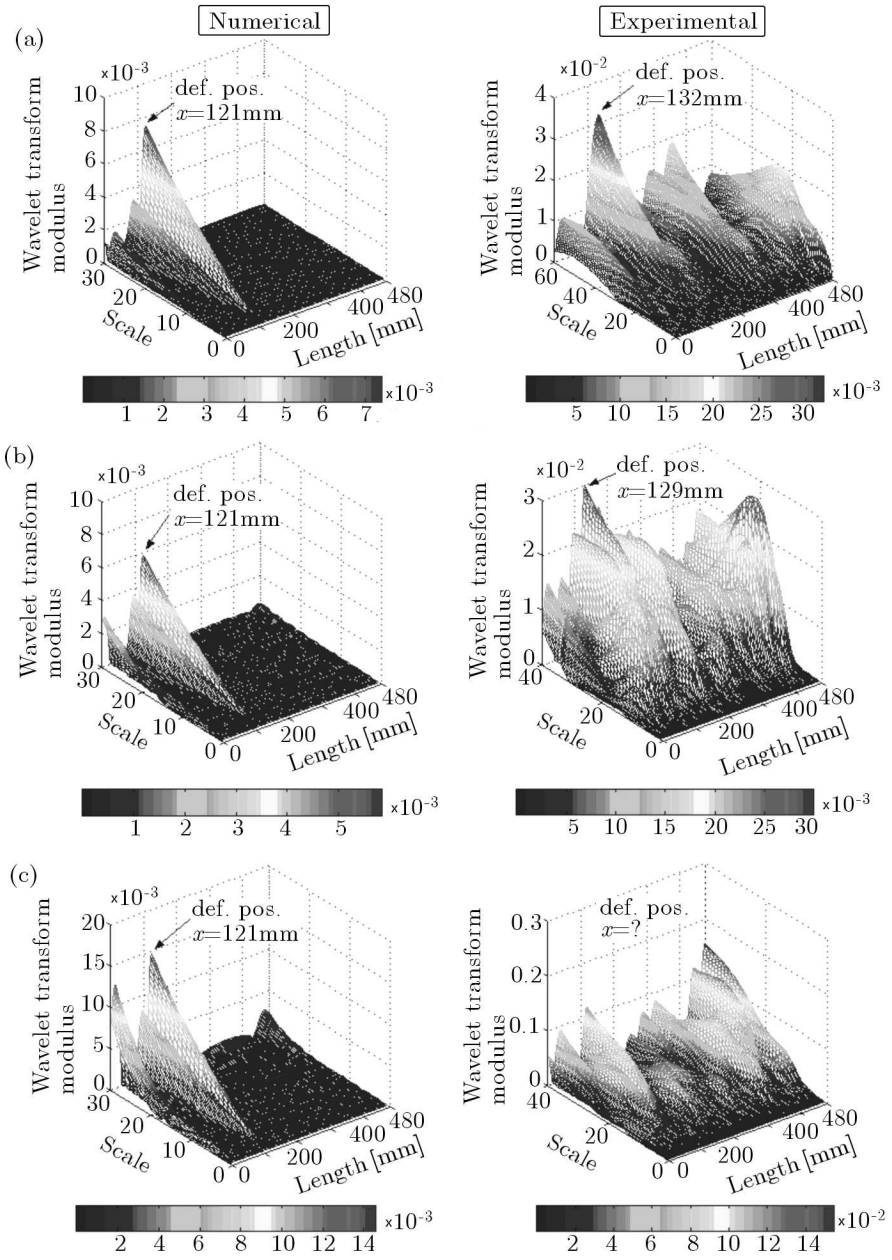

Fig. 11. Wavelet transform modulus of the beam numerical and experimental mode shapes: (a) first, (b) second, (c) third

data are capable to indicate location of the defect. The real defect position is $x = 240$ mm and $y = 240$ mm and it is in agreement with the recognition of the defect position equal to $x = 240$ mm and $y = 243$ mm. Analysis of the second and third mode shapes was performed using gaus4 wavelet along the plate width, and gaus6 wavelet along the plate length. The numerical results enable one to identify defect position, however in the case of the experimental data the noise masks the defect position.

In the last example, the wavelet analysis is conducted on three mode shapes of the cylindrical shell. Gaussian wavelet gaus6 is considered. The one-dimensional CWT of the numerical and experimental mode shapes (Fig. 13) is performed for scales $s = 1$-10. In the case of the numerical data, the maximum modulus grows with the increase of the scale and clearly points to the damage position at 288 mm. The CWT results based on the experimental third mode shape (Fig. 13c) have additional maxima lines resulting from the measurement noise. Nevertheless, the constant slope of the maximum line clearly indicates the damage location at 298 mm. Wavelet transforms of the first and second experimental mode shapes do not allow for detection of the defect position (Figs. 13a and 13b).

5.3. Predictions of NW system

The NW damage identification ability has been tested on the experimental beam, plate and shell mode shapes described in Section 5.1. In the case of the beam and shell mode shapes, selected lines of the wavelet transform modulus were used as inputs. The set of data for the beam consisted of 3 patterns. For the beam first mode shape, the wavelet transform modulus computed for scale $s = 60$ was used, whereas for the second and third modes, the wavelet transform modulus computed for the scale $s = 40$ was applied. For the shell, the set of input data consisted of 3 patterns, calculated for the scale $s = 10$. In the case of plate, the two-dimensional wavelet transform moduli were converted into a one-dimensional input signal since lines at different locations can be treated separately. In this simulation, only the lines passing through the centre of the defect have been considered. The set of the experimental input data consists of 6 patterns, i.e. 3 patterns along the length of the plate and 3 patterns along the width of the plate. The results are plotted in Fig. 14. It is visible that all patterns are in agreement with the actual values with the correlation coefficient equal to 0.95247. The detailed values for all examples are contained in Table 4.

The defect presence identification by the CWT was possible only for 5 of 12 input patterns. The NW system prediction was completely successfully for

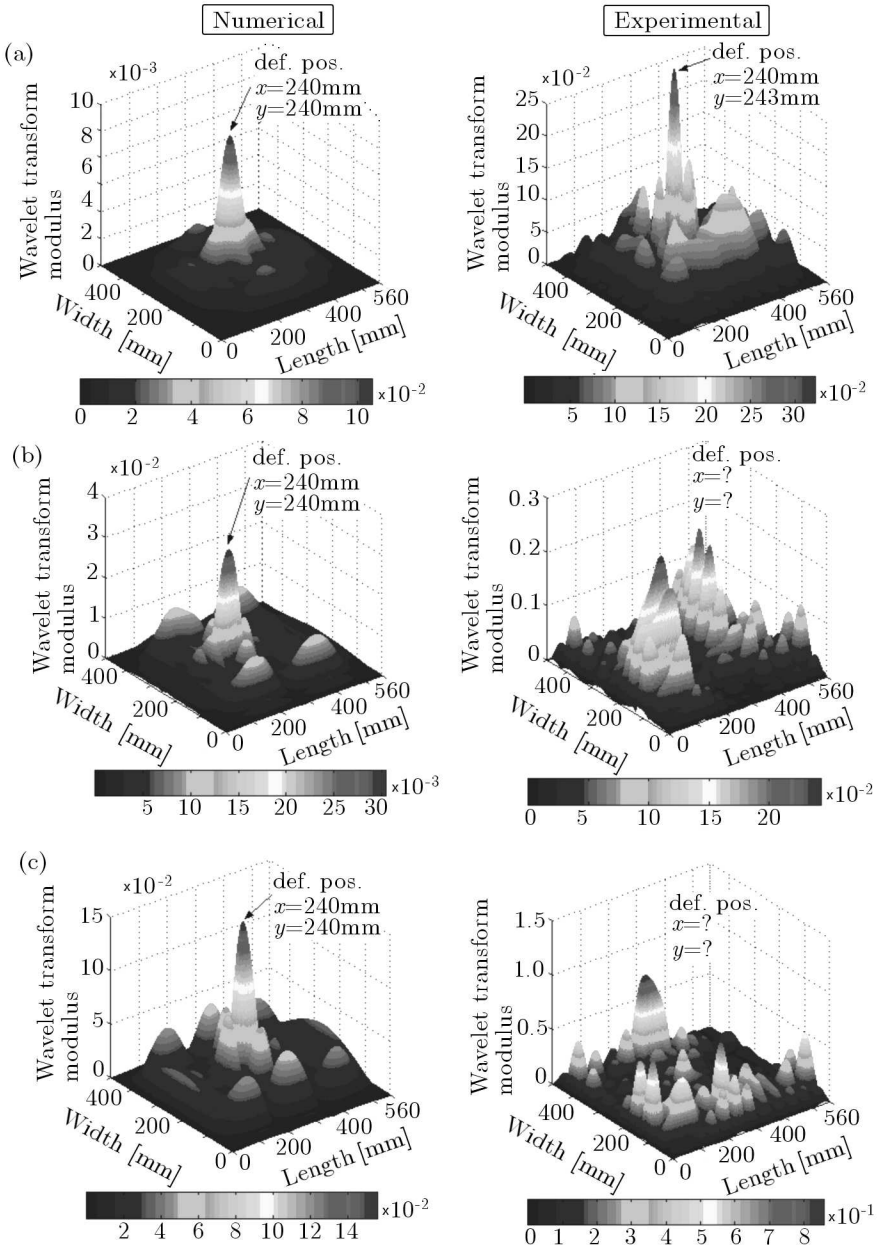

Fig. 12. Wavelet transform modulus of the plate numerical and experimental mode shapes: (a) first, (b) second, (c) third

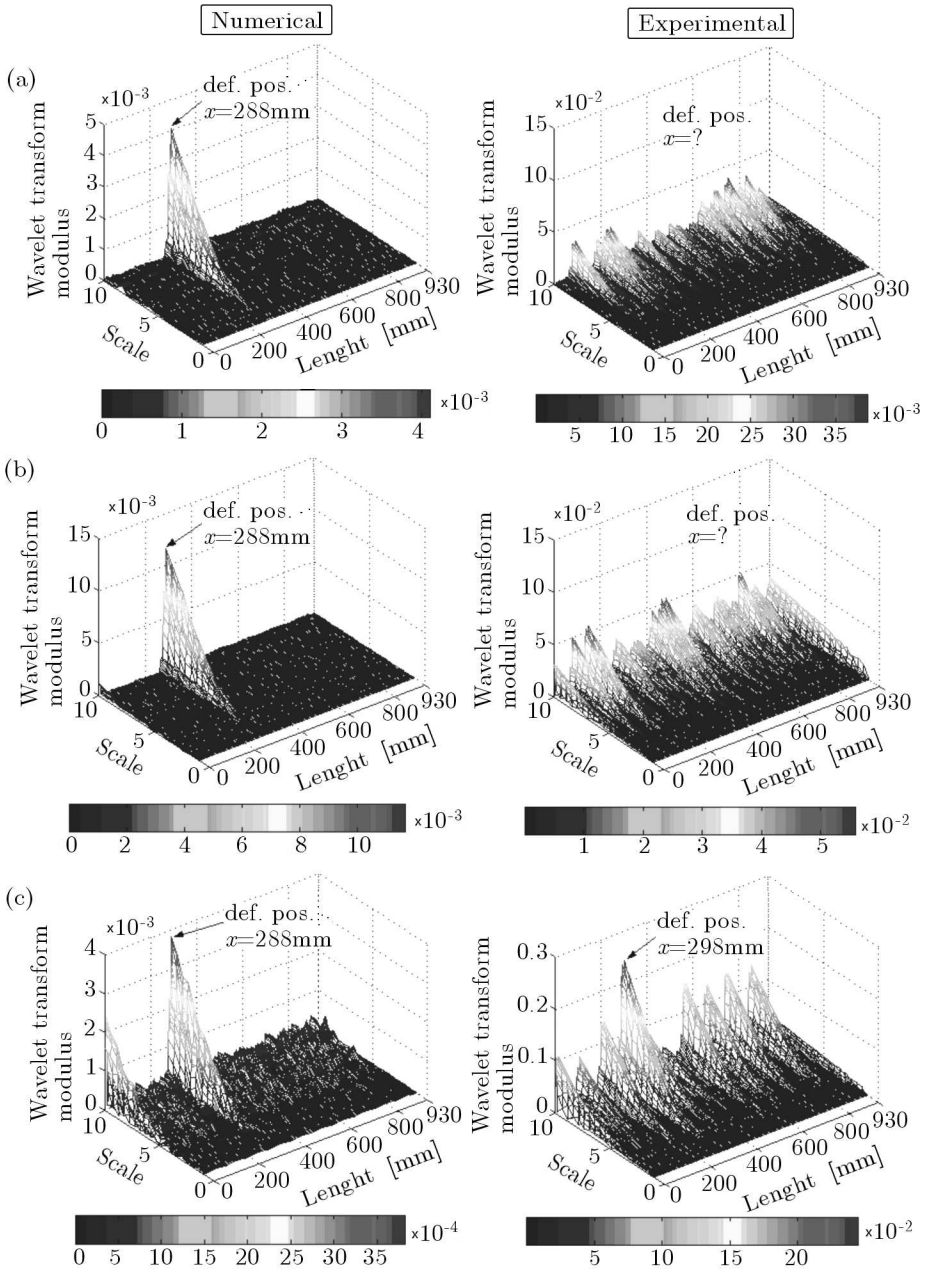

Fig. 13. Wavelet transform modulus of the shell numerical and experimental mode shapes: (a) first, (b) second, (c) third

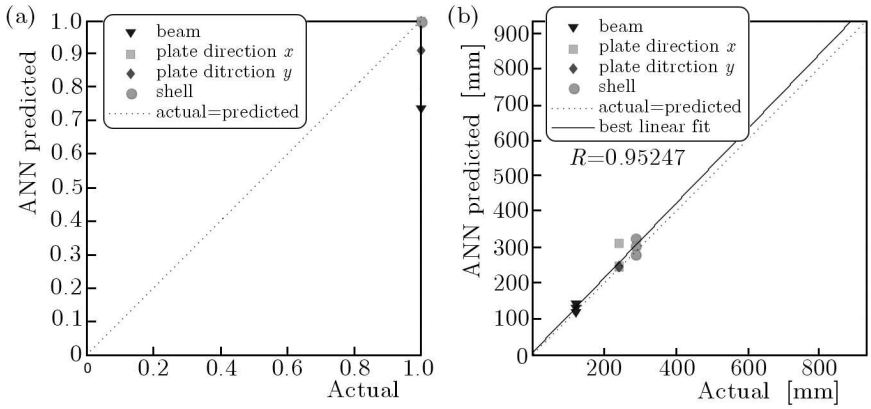

Fig. 14. Results of the NW system for the experimental beam, plate and shell mode shapes; (a) crack presence, (b) crack localization

Table 4. Actual, recognized by wavelets and neurally predicted defect identification

Structure	Input patterns	Patterns description	Defect presence			Defect centre position [mm]		
			Actual	Recog. by CWT	Predicted by ANN	Actual	Recog. by CWT	Predicted by ANN
beam	mode 1	gaus4, $s = 60$	1	1	0.9892	121	132	143.9611
	mode 2	gaus6, $s = 40$	1	1	0.9931	121	129	130.5971
	mode 3	gaus6, $s = 40$	1	–	0.7371	121	–	118.4275
plate (along x)	mode 1	gaus4, $s = 40$	1	1	0.9983	240	240	243.0938
	mode 2	gaus6, $s = 40$	1	–	1.0043	240	–	311.3410
	mode 3	gaus6, $s = 40$	1	–	0.9994	240	–	246.5563
plate (along y)	mode 1	gaus4, $s = 40$	1	1	0.9998	240	243	244.9450
	mode 2	gaus4, $s = 40$	1	–	0.9993	240	–	243.3374
	mode 3	gaus4, $s = 40$	1	–	0.9127	240	–	247.6269
shell	mode 1	gaus6, $s = 10$	1	–	0.9978	287.5	–	325.7603
	mode 2	gaus6, $s = 10$	1	–	0.9987	287.5	–	303.4104
	mode 3	gaus6, $s = 10$	1	1	0.9981	287.5	298	280.7378

10 patterns (with difference ranging from 0.02% to 1.08%) and quite successfully for 2 patterns (with difference 8.73% and 26.27%). The NW system could identify the damage presence in all the considered cases with the average error of 3.17%.

The identification of defect position by the CWT was also possible only for 5 of 12 input patterns. The errors of the CWT based peak-picking method reach from 0% to 9.09%. The NW was able to predict defect localization for all cases, including cases, in which it was impossible to locate the defect by the CWT. The NW prediction was successful for 9 patterns (with difference ranging from 1.29% to 7.93%) and satisfactory for 3 patterns (with differences 13.31%, 18.98% and 29.73%). The NW system could indicate damage location in all the considered cases with the average error of 7.55%.

6. Conclusions

In this paper, the neuro-wavelet damage detection method for defect identification is presented. The technique is studied on experimental mode shapes of beam, plate and shell structures. The search for the defect location, conducted by picking the largest wavelet transform modulus, is enhanced by the artificial neural network. A simple, backpropagation neural network was trained on static deflection lines of the cantilever beam. Although, the network was taught on the static data, it could effectively localize the damage of the same type in more complex structures, like plate or shell.

The results of the wavelet damage detection and analysis of the neural network simulations lead to the following conclusions:

- The wavelet damage detection method might be suitable for detecting relatively small damage (with damage area being 0.2% of the total shell area). In more complex structures, the sensitivity of higher modes to small defects might be high (the shell highest considered mode appeared the best for damage detection).
- The NW system can predict damage location with relatively good precision even for the cases with no visible peaks in the wavelet transforms.
- The NW system for a complex engineering object can be trained on data obtained on a simple structure. In such a case, it is easy to conduct an experiment and numerical simulations to collect the ANN training data.
- The reliability of the NW system prediction can be improved by application of a more advanced ANN architecture and the use of a large number of training patterns corresponding to the cases encountered in the real structures.
- The artificial neural network solutions belong to the class of the so-called soft computing and the ANN can predict defects only with a certain probability. Hence, the application of the ANN provides sometimes worse

identification of defect positions than the identification of defect localizations by CWT. Nevertheless, the ANN predictions are relatively good in the cases when it is impossible to locate the defect by analysis of the wavelet transforms of mode shapes.

- The system supporting the decision making process on damage location should not rely solely on the neural network. The ANN gives only a probable damage location while the peak-picking method, if applicable, provides reliable results. The system should combine the results obtained by both methods.

References

1. Barai S.V., Pandey P.C., 1997, Time-delay neural networks in damage detection of railway bridges, **Advanced in Engineering Software**, **28**, 1-10
2. Bow S.-T., 2002, *Pattern Recognition and Image Preprocessing. Marcel Dekker*, Inc., New York
3. Cabell R.H., Fuller C.R., O'Brien W.F., 1998, Neural network modeling of oscillatory loads and fatigue damage estimation of helicopter components, *Journal of Sounds and Vibration*, **209**, 329-342
4. Chang C.-C., Chen L.-W., 2004, Damage detection of a rectangular plate by spatial wavelet based approach, *Applied Acoustic*, **65**, 819-832
5. Demuth H., Beale M., 2003, *Neural Network Toolbox User's Guide*, The MathWorks, Inc.
6. Douka E., Loutridis S., Trochidis A., 2003, Crack identification in beams using wavelet analysis, *International Journal of Solids and Structures*, **40**, 3557-3569
7. Douka E., Loutridis S., Trochidis A., 2004, Crack identification in plates using wavelet analysis, *Journal of Sound and Vibration*, **270**, 279-295
8. Garg A.K., Mahapatra D.R., Suresh S., Gopalakrishnan S., Omkar S.N., 2004, Estimation of composite damage model parameters using spectral finite element and neural network, *Composites Science and Technology*, **64**, 2477-2493
9. Gentile A., Messina A., 2003, On the continuous wavelet transforms applied to discrete vibrational data for detecting open cracks in damaged beams, *International Journal of Solids and Structures*, **40**, 295-315
10. Hoła J., Schabowicz K., 2005, New technique of nondestructive assessment of concrete strength using artificial intelligence, *NDT&E International*, **38**, 251-259

11. HONG J.-C., KIM Y.Y., LEE H.C., LEE Y.W., 2002, Damage detection using Lipschitz exponent estimated by the wavelet transform: applications to vibration modes of beam, *International Journal of Solids and Structures*, **39**, 1803-1846

12. HU Y.H., HWANG J.-N., 2002, *Handbook of Neural Networks Signal Processing*, CRC Press LLC

13. KAO C.Y., HUNG S.-L., 2003, Detection of structural damage via free vibration responses generated by approximating artificial neural networks, *Computer and Structures*, **81**, 2631-2644

14. KUŹNIAR K., WASZCZYSZYN Z., 2002, Neural analysis of vibration problems of real flat buildings and data pre-processing, *Engineering Structures*, **24**, 1327-1335

15. LIU S.W., HUANG J.H., SUNG J.C., LEE C.C., 2002, Detection of cracks using neural networks and computational mechanics, *Computer Methods in Applied Mechanics and Engineering*, **191**, 2831-2845

16. MALLAT S., 1998, *A Wavelet Tour of Signal Processing*, Academic Press

17. MOLLER M.F., 1993, A scaled conjugated gradient algorithm for fast supervised learning, *Neural Networks*, **6**, 525-533

18. OKAFOR A.C., DUTTA A., 2001, Optimal ultrasonic pulse repetition rate for damage detection in plates using neural networks, *NDT&E International*, **34**, 469-481

19. RUCKA M., WILDE K., 2005, Damage location in beam and plate structures by wavelet analysis of experimentally determined mode shapes, *Key Engineering Materials*, 293/294, 313-320

20. RUCKA M., WILDE K., 2006a, Application of continuous wavelet transform in vibration based damage detection method for beam and plates, *Journal of Sound and Vibration*, **297**, 536-550

21. RUCKA M., WILDE K., 2006b, Crack identification using wavelets on experimental static deflection profiles, *Engineering Structures*, **28**, 279-288

22. RUCKA M., WILDE K., 2007, *Application of Wavelet Analysis in Damage Detection and Localization*, Wydawnictwo Politechniki Gdańskiej

23. SAHIN M., SHENOI R.A., 2003, Quantification and localization of damage in beam-like structures by using artificial neural networks with experimental validation, *Engineering Structures*, **25**, 1785-1802

24. SANZ J., PERERA R., HUERTA C., 2007, Fault diagnosis of rotation machinery based on auto-associative neural networks and wavelet transforms, *Journal of Sound and Vibration*, **302**, 981-999

25. WANG Q., DENG X., 1996, Damage detection with spatial wavelets, *International Journal of Solids and Structures*, **36**, 3443-3468

26. WASZCZYSZYN Z., ZIEMIAŃSKI L., 2001, Neural networks in mechanics of structures and materials – new results and prospects of application, *Computer and Structures*, **79**, 2261-2276

27. WILDE K., HIRSZ M., DUDEK M., RUCKA M., 2006, Experimental study on multilevel damage detection strategy for plate structures, *Proceedings of the Forth World Conference on Structural Control and Monitoring*, San Diego

28. YAM L.H., YAN Y.J., JIANG J.S., 2003, Vibration-based damage detection for composite structures using wavelet transform and neural identification, *Composite Structures*, **60**, 403-412

29. YEUNG W.T., SMITH J.W., 2005, Damage detection in bridges using neural networks for pattern recognition of vibration signatures, *Engineering Structures*, **27**, 685-698

30. YUN C.-B., YI J.-H., BAHNG E.Y., 2001, Joints damage of framed structures using a neural networks technique, *Engineering Structures*, **23**, 425-435

31. ZACHARIAS J., HARTMANN C., DELGADO A., 2004, Damage detection on crates of beverages by artificial neural networks trained with finite-element data, *Computer Methods in Applied Mechanics and Engineering*, **193**, 561-574

32. ZAPICO J.L., GONZÁLEZ M.P., WORDEN K., 2003, Damage assessment using neural networks, *Mechanical Systems and Signal Processing*, **17**, 119-125

33. ZUBAYDI A., HADDARA M.R., SWAMIDAS A.S.J., 2002, Damage identification in a ship's structure using neural networks, *Ocean Engineering*, **29**, 1187-1200

Wykrywanie uszkodzeń w konstrukcjach belkowych, płytowych i powłokowych przy użyciu systemu neuro-wavelet

Streszczenie

Niniejsza praca poświęcona jest technice diagnostyki konstrukcji bazującej na transformacie falkowej oraz sztucznych sieciach neuronowych (tzw. system neuro-wavelet). Zastosowanie analizy falkowej pozwala na lokalizację uszkodzeń wymagającą minimalnej ilości danych wejściowych. W tym celu niezbędna jest tylko odpowiedź konstrukcji pomierzona w wielu punktach. Poprawę efektywności lokalizacji zniszczeń uzyskano poprzez użycie sztucznej sieci neuronowej. Nauczona sieć neuronowa poprawnie rozpoznaje miejsce położenia uszkodzeń, nawet w przypadkach, gdy określenie położenia uszkodzenia nie było możliwe bezpośrednio z obliczonych współczynników falkowych. Zaproponowana metoda została sprawdzona eksperymentalnie na przykładach konstrukcji belkowych, płytowych i powłokowych.

Manuscript received October 4, 2009; accepted for print December 2, 2009